remote sensing

MDPI

Article

Spatiotemporal Patterns of Vegetation Evolution in a Deep Coal Mining Subsidence Area: A Remote Sensing Study of Liangbei, China

Weitao Yan [1,2,*], Zhiyu Chen [1], Junjie Chen [1] and Chunsu Zhao [1]

[1] School of Surveying and Land Information Engineering, Henan Polytechnic University, Jiaozuo 454000, China; 212204010034@home.hpu.edu.cn (Z.C.); 212204010039@home.hpu.edu.cn (C.Z.)
[2] State Collaborative Innovation Center of Coal Work Safety and Clean-Efficiency Utilization, Henan Polytechnic University, Jiaozuo 454003, China
* Correspondence: yanweitao@hpu.edu.cn

Abstract: This study aims to provide a comprehensive analysis of the impacts of high-intensity coal mining on vegetation in Liangbei Town, a typical deep coal mining area in central of China. Using Landsat remote sensing data from 2000 to 2023, processed by the Google Earth Engine (GEE) platform, the study calculates the Normalized Difference Vegetation Index (NDVI). Temporal and spatial distribution patterns of vegetation were assessed using LandTrendr algorithm, Sen's slope estimation, the Mann–Kendall test, the coefficient of variation, and the Hurst index. Vegetation growth dynamics were further analyzed through transfer matrix and intensity analysis frameworks. Driving factors influencing vegetation trends were evaluated using local climate data and surface deformation variables from SAR imagery. Temporal Dimension: From 2000 to 2023, the annual NDVI in Liangbei Township showed an upward trend with a growth rate of 0.0894 $(10a)^{-1}$, peaking at 0.51 in 2020. Spatial Dimension: The NDVI distribution in Liangbei Township displayed a pattern of being lower in the center and higher around the edges, with values concentrated between 0.4 and 0.51, covering 50.34% of the total area. Trend of Change: Between 2000 and 2023, 83.28% of the area in Liangbei Township experienced significant improvement in the NDVI, with vegetation growth trends shifting primarily from slight to significant improvement, encompassing a total area of 10.98 km². This shift exhibited a marked tendency. Driving Factors: Deep mining in Liangbei Township is concentrated in the eastern part, with SAR imagery indicating a maximum surface subsidence of 0.26 m. As surface subsidence increases, the NDVI significantly decreases. The findings suggest that in the future, 91.13% of the vegetation in Liangbei Township will display an antipersistent change trend. The study offers critical insights into the interaction between mining activities and vegetation cover can serve as a reference for environmental evolution and management in similar mining areas.

Keywords: deep mining; ecological monitoring; Mann–Kendall test; intensity analysis framework

Citation: Yan, W.; Chen, Z.; Chen, J.; Zhao, C. Spatiotemporal Patterns of Vegetation Evolution in a Deep Coal Mining Subsidence Area: A Remote Sensing Study of Liangbei, China. *Remote Sens.* **2024**, *16*, 3204. https://doi.org/10.3390/rs16173204

Academic Editors: Yuanheng Sun, Huazhong Ren and Chengye Zhang

Received: 16 July 2024
Revised: 20 August 2024
Accepted: 27 August 2024
Published: 29 August 2024

1. Introduction

The central and eastern regions of China are currently witnessing a shift toward deep mining, with underground coal resources being extracted from depths reaching up to a kilometer [1,2]. While the continuous, large-scale extraction of these deep underground resources has significantly contributed to regional economic growth, it has also exacerbated ecological degradation, particularly affecting surface vegetation and local ecosystems [3,4]. Previous research has established a clear link between underground mining and ecological disruption. For instance, Wang Shuangming et al. [5] introduced the concept of ecological water level to elucidate the impact of mining activities on surface vegetation, while Li Shuzhi et al. [6] provided ecological restoration strategies tailored for high groundwater-level plain mining areas. Similarly, Yue Hui et al. [7] utilized remote sensing ecological

indices to reveal the spatiotemporal dynamics of ecological changes in the Shendong mining area, and Hu Haifeng et al. [8] examined the degradation characteristics in coal mining subsidence regions within the loess hilly areas of Shanxi, proposing restoration techniques specific to these fragile environments. These studies collectively highlight the multifaceted impacts of deep coal mining on surface ecosystems and outline various approaches for reducing these effects.

Vegetation serves as a critical indicator of surface ecological health, making it a valuable proxy for assessing the environmental consequences of underground mining activities [9–11]. Traditional vegetation monitoring methods in mining areas, typically reliant on field sampling, have proven to be limited in scope due to their labor-intensive, time-consuming nature and their inherent inability to cover large geographic areas [12–14]. In contrast, remote sensing technology offers a superior alternative, characterized by its extensive spatial coverage [15], capability for all-weather observation [16], and long-term temporal monitoring capacity [17,18]. Remote sensing-derived vegetation indices, such as the Normalized Difference Vegetation Index (NDVI), have been extensively employed by researchers to quantitatively evaluate changes in vegetation cover within mining regions [19–21]. However, conventional analysis techniques predominantly focus on monotonic trends and smooth transitions within long-term time series data, often employing transition matrices to understand vegetation dynamics [22]. These methods typically assess area-based changes [23–25], but they fail to account for the intensity and variability in vegetation growth trends, thereby overlooking the nuanced effects of ecological restoration efforts and the resilience of vegetation in response to mining-induced disturbances.

Given these limitations, this study addresses the need for a more comprehensive approach by incorporating an intensity analysis framework alongside conventional methods. The framework not only captures the shifts in vegetation growth trends but also identifies the ways in which this transformation presents itself. By doing so, it provides a more nuanced understanding of the relationship between mining activities and ecological outcomes, specifically in the context of ecological restoration projects.

To achieve this, Liangbei was selected as a case study, representing a typical area undergoing deep mining in central of China. Utilizing the Google Earth Engine (GEE) platform, this research constructs a detailed NDVI dataset spanning from 2000 to 2023. Analytical techniques such as the LandTrendr algorithm, Sen's slope estimation, the Mann–Kendall (MK) test, coefficient of variation, and the Hurst index are employed to explore the spatiotemporal evolution of vegetation under deep mining conditions. Additionally, the intensity analysis framework is introduced to examine shifts in vegetation growth trends across two distinct periods: 2000–2012 and 2012–2023. This study also incorporates D-InSAR technology to assess the impact of underground mining activities on surface vegetation, thereby providing critical insights into the driving mechanisms behind these changes.

2. Materials and Methods

2.1. Study Area

Liangbei Township is located southwest of Yuzhou City in Henan Province, China. covering the mines of China Xinliang Mining Company Limited, China Shenhuo Wenyu Mining Company Limited, China Pingyu Coal and Electricity Company Limited's four mines, China Henan Shenhuo Group Company Limited and many other deep mining mines. The geographical coordinates are 113°24′0″~113°28′0″E and 34°4′0″~34°8′0″N, with a total area of about 43.8 km^2. It is situated in the southern foothills of the Taihang Mountains system, north of the Huaihe River Plain, characterized by higher elevations in the west and lower elevations in the east. The climate is warm temperate continental semi-arid, with moderate temperatures and distinct seasons (Figure 1). The main soil type in this area is drab soil. The region holds proven coal reserves of 290 million tons. The coal seams are simple and stable, with a mining depth exceeding 500 m. The thickness of the coal seams ranges from 2.8 to 7 m, with an average thickness of 5.04 m. The mining operations employ single-level uphill mining, fully mechanized mining techniques with

large mining heights, and long-wall coal mining technology, using the caving method for roof management.

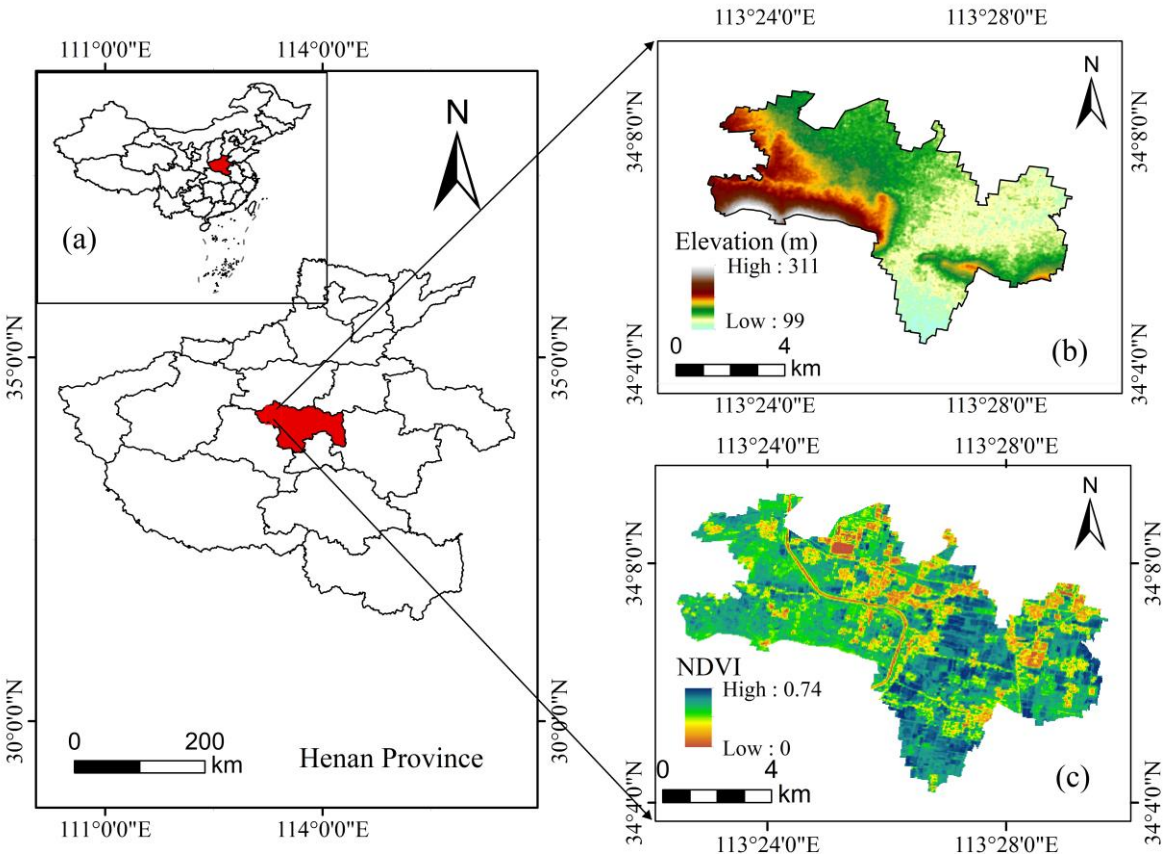

Figure 1. Location of Liangbei Township. (**a**) Location, (**b**) elevation, (**c**) NDVI.

2.2. Data Sources and Preprocessing

The remote sensing data utilized in this study were sourced from the Landsat 5, 7, and 8 satellites, provided by the United States Geological Survey (USGS). The data, spanning from 2000 to 2023, were obtained as Landsat T1_L2 products by the Google Earth Engine. The images have a spatial resolution of 30 m [26] and a temporal resolution of 16 days [27]. The images passing atmospheric correction, radiometric calibration, and cloud removal during preprocessing [28]. For the striping data loss issue inherent to Landsat 7 images, a destriping function was employed to process the data. Subsequently, the Normalized Difference Vegetation Index (NDVI) was computed online, and the images were synthesized using a median composite algorithm [29]. The image cropping was also performed online using the Quality Mosaic algorithm to further mitigate adverse effects caused by clouds, atmospheric conditions, and satellite sensor angles.

The Sentinel-1 twin-satellite system is part of the Copernicus program, launched by the European Commission (EC) and the European Space Agency (ESA). This system consists of the Sentinel-1A and Sentinel-1B polar-orbiting satellites, which are in the same orbit with a 180° phase difference. This study utilized Sentinel-1A SAR SLC data, which is available from NASA's website, to obtain surface deformation measurements. The spatial resolution of this data is 5 m × 20 m [30] and a revisit period of 12 days [31]. A total of 120 SAR SLC images were acquired from 2018 to 2023. The D-InSAR technique was used to process the images to derive surface subsidence values. The processing steps included baseline estimation, interferogram generation [32], removal of topography and flat-earth phase [33], interferogram filtering, phase unwrapping, phase-to-deformation conversion, and geocoding [34].

2.3. Technological Route

This research aims to investigate the spatiotemporal evolution of vegetation cover in Liangbei, China, a deep coal mining subsidence area, from 2000 to 2023. Using NDVI data processed on the GEE platform, this study identifies trends and drivers of vegetation changes under the influence of mining activities. The analysis is structured into the following steps (Figure 2):

(1) Data Collection and Preprocessing: Compile Landsat 5, 7, 8 and Sentinel-1 data for Liangbei Township. Calculate NDVI values using the Google Earth Engine (GEE) platform. Acquisition of surface deformation values by processing Sentinel-1 data with SARscape_v560 software. Address missing data through interpolation techniques to ensure continuity.

(2) Trend Analysis: Calculate the coefficient of variation (CV) to evaluate the stability of vegetation cover across the study period. Apply LandTrendr algorithm, Sen's slope estimator, and Mann–Kendall trend test to determine trends in NDVI data. Use the transition matrix and intensity analysis framework to examine shifts in vegetation growth patterns over time.

(3) Driving Factor Analysis: Correlate NDVI trends with meteorological data and ground subsidence data derived from SAR imagery. Identify the key drivers of vegetation change, emphasizing the role of deep coal mining and its associated environmental impacts.

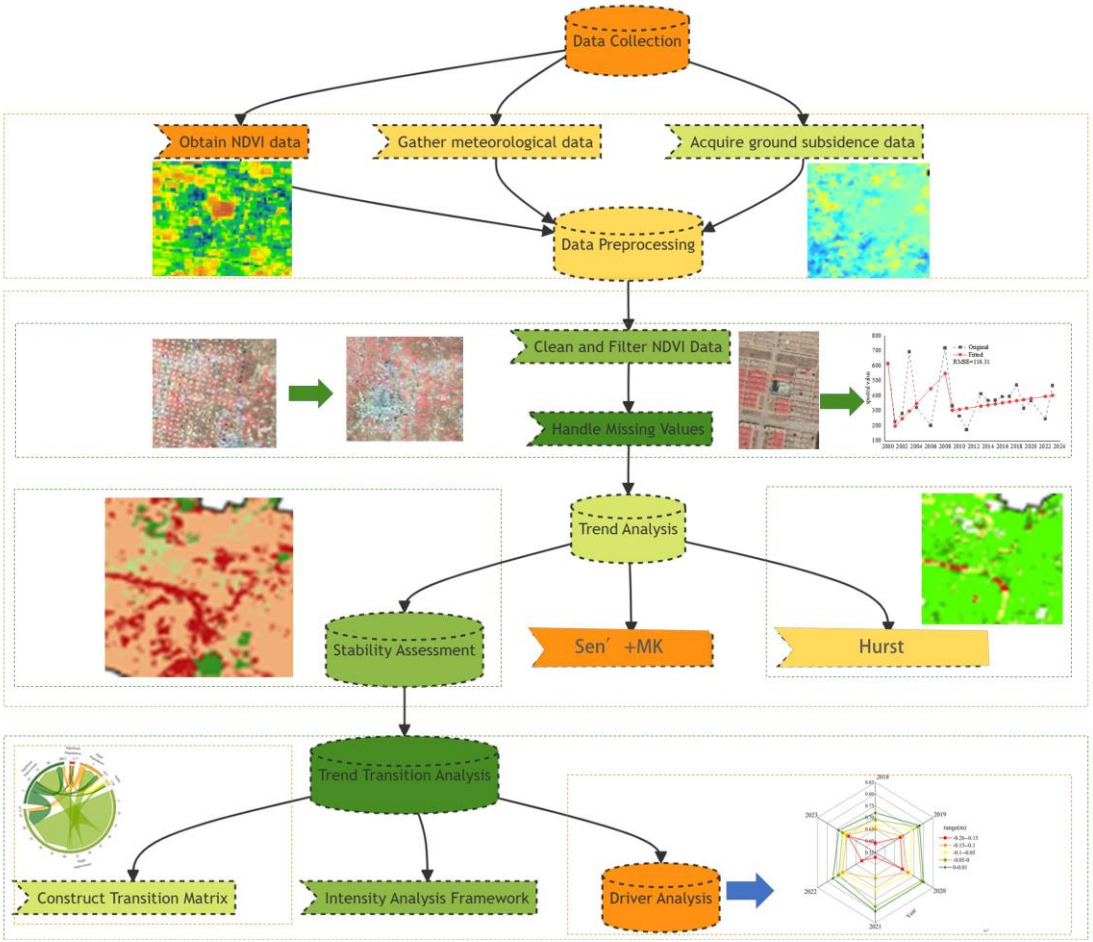

Figure 2. Flow chart of the study.

2.4. Method

2.4.1. Normalized Difference Vegetation Index

The Normalized Difference Vegetation Index (NDVI) is a crucial parameter reflecting vegetation growth and nutritional status [35]. This index can indicate the influence of the plant canopy's background, including soil, wet ground, snow, dead leaves, and roughness, all of which are related to vegetation cover. The calculation formula for NDVI is as follows:

$$NDVI = \frac{\rho_{NIR} - \rho_R}{\rho_{NIR} + \rho_R} \quad (1)$$

where ρ_{NIR} represents the spectral reflectance in the near-infrared band and ρ_R represents the spectral reflectance in the red band. The resulting NDVI values range from $[-1, 1]$, with higher values indicating more vegetation cover on the surface [36].

2.4.2. LandTrendr Algorithm

This study employs the LandTrendr algorithm to identify disturbances and recovery patterns in the NDVI time series for typical land cover in Liangbei Town. The LandTrendr algorithm is designed to capture both gradual and abrupt changes within the time series by using fitting or smoothing techniques to minimize background noise [37]. This process generates a trajectory of time series imagery that accurately reflects temporal changes in the landscape. The algorithm is particularly effective in detecting subtle differences, capturing abrupt events, and performing per-pixel analysis of time series spectral data, which helps extract detailed information regarding changes in land cover characteristics.

By analyzing the sequence and duration of disturbances and recovery, the LandTrendr algorithm provides valuable insights into the resilience of vegetation and the long-term effects of anthropogenic activities, such as mining [38]. This capability is crucial for understanding how different land cover types respond to environmental changes over time, especially in regions like Liangbei, where intensive land use practices significantly influence the landscape.

2.4.3. Coefficient of Variation

In this study, the coefficient of variation (CV) for each pixel was calculated using NDVI time series data from 2003 to 2022. The CV is a statistical measure used to describe the degree of dispersion in data [39]. A higher CV value indicates greater dispersion in the data series. The calculation method is as follows:

$$CV = \frac{\sigma}{\mu} \quad (2)$$

where σ is the standard deviation of the NDVI values and μ is the mean of the NDVI values over the time series. The classification criteria are as follows: 0–0.1 indicates stability; 0.1–0.2 indicates relative stability; 0.2–0.3 indicates instability; and values above 0.3 indicate extreme instability.

2.4.4. Theil–Sen Slope Estimation and Mann–Kendall Test

The trends in NDVI changes in Liangbei Town were analyzed using the Theil–Sen estimator and Mann–Kendall test. The Theil–Sen slope estimator is a robust non-parametric statistical method for trend analysis [40], suitable for long-term time series data [41]. The calculation formula is as follows:

$$\beta = Median\left(\frac{x_j - x_i}{j - i}\right) \forall j > i \quad (3)$$

where *Median ()* represents the median value. If $\beta > 0$, it indicates an increasing NDVI trend, and if $\beta < 0$, it indicates a decreasing NDVI trend.

The Mann–Kendall test, also known as the MK test, can test not only the trend of the time series [42], but also whether the time series has experienced a mutation [43]. The calculation formula is as follows:

$$\mathrm{sgn}(x - x) = \begin{cases} +1 & x_j - x_i > 0 \\ 0 & x_j - x_i = 0 \\ -1 & x_j - x_i < 0 \end{cases} \quad (4)$$

$$S = \sum_{i=1}^{n-1} \sum_{j=i+1}^{n} \mathrm{sgn}(x_j - x_i) \quad (5)$$

$$Z = \begin{cases} \frac{S}{\sqrt{Var(S)}} & (S > 0) \\ 0 & (S = 0) \\ \frac{S+1}{\sqrt{Var(S)}} & (S < 0) \end{cases} \quad (6)$$

$$Var = \frac{n(n-1)(2n+5)}{18} \quad (7)$$

where x_j and x_i refer to NDVI time series; *sgn* represents the sign function; S denotes the test statistic; Z is the standardized test statistic; n is the number of data points. At a given significance level a, if $|Z| > Z_{1-\alpha/2}$, it suggests the presence of a significant trend change. In this study, a is set as to 0.05, implying the evaluation of the significance of NDVI time series changes at a 0.05 significance level.

2.4.5. Hurst Exponent

The Hurst exponent is used in this study to describe the future pixel-wise change trends in Liangbei. The Hurst exponent is based on the rescaled range (R/S) analysis method [44] and serves as an indicator to determine whether a time series follows a random walk or a biased random walk process [45]. The calculation method is as follows:

For a given time series $\{NDVI(t), t = 1, 2, \ldots, n\}$, the mean sequence is defined as:

$$\overline{NDVI_{(T)}} = \frac{1}{T} \sum_{t=1}^{T} NDVI_{(T)} \ldots T = 1, 2, \ldots, n \quad (8)$$

The cumulative deviation is:

$$X_{(t,T)} = \sum_{t=1}^{t} \left(NDVI_{(t)} - \overline{NDVI_{(T)}} \right) \ldots 1 \leq t \leq T \quad (9)$$

The standard deviation is:

$$S_{(T)} = \left[\frac{1}{T} \sum_{t=1}^{T} \left(NDVI_{(t)} - NDVI_{(T)} \right)^2 \right]^{\frac{1}{2}} \ldots T = 1, 2 \ldots, n \quad (10)$$

Then, based on the above formulas, we obtain:

$$\frac{R(t)}{S(t)} \propto T^H \quad (11)$$

If the sequence to be analyzed exhibits the Hurst phenomenon, the Hurst exponent H can be estimated using the relationship:

$$log(\frac{R(t)}{S(t)}) = \alpha + Hlog(t) \quad (12)$$

The least squares method is used for fitting to obtain H

If $0 < H < 0.5$, it indicates antipersistence in the NDVI time series of Liangbei Town, meaning the future trend is opposite to the past trend [46]. The closer H is to 0, the stronger the antipersistence.

If $0.5 < H < 1$, it indicates persistence in the NDVI time series, meaning the future trend is similar to the past trend [47]. The closer H is to 1, the stronger the persistence. $H = 0.5$, it suggests that the NDVI changes in Liangbei Town follow a random process with no apparent persistence within the time series.

2.4.6. Intensity Analysis Framework

The intensity analysis in this study is focused on assessing changes in vegetation growth trends over different time intervals. Two key measures are used: absolute intensity and relative intensity.

Absolute intensity reflects the absolute quantity of vegetation growth trend changes over a specified time interval. It analyzes the transition of one type of vegetation growth trend to another and vice versa. For the time interval [Tt, $Tt + 1$], the absolute transition intensity AI_{in} is the area where an initial vegetation growth trend type i changes to a final growth trend type n (Equation (13)). The mean absolute transition intensity MAI_n is the average of all transitions to type n from other types (Equation (14)).

$$AI_{in} = \frac{C_{in}}{C_{nn}} \tag{13}$$

$$MAI_n = \frac{1}{I-1}\sum_{i \neq n} AI_{in} \tag{14}$$

where i represents the initial vegetation growth trend code, n represents the final vegetation growth trend type code, C_{in} is the area of vegetation growth trend i transitioning to trend n during the interval [Tt, $Tt + 1$], C_{nn} is the area of trend n that remains unchanged during the interval [Tt, $Tt + 1$], t represents the initial time node code, Tt represents the year corresponding to the initial time node, $Tt + 1$ represents the year corresponding to the final time node, and I is the number of initial vegetation growth trend types.

Relative intensity further analyzes the intensity of transitions between vegetation growth trends based on absolute intensity. The relative transition intensity RI_{in} is the proportion of the initial vegetation growth trend i transitioning to the final growth trend n during the interval [Tt, $Tt + 1$] (Equation (15)). The mean relative transition intensity MRI_n is the average proportion of all transitions to trend n from other types (Equation (16)).

$$RI_{in} = \frac{C_{in}}{\sum_{j \neq n} C_{ij}} \tag{15}$$

$$MRI_n = \frac{1}{I-1}\sum_{i \neq n} RI_{in} \tag{16}$$

where C_{ij} represents the area of the initial vegetation growth trend type i transitioning to the final growth trend type j during the interval [Tt, $Tt + 1$] and C_{nj} represents the area of the vegetation growth trend type n transitioning to the final growth trend type j.

Equation (17) calculates the relative transition out intensity RO_{mj} for an initial vegetation growth trend type m transitioning to a final growth trend type j during the interval [Tt, $Tt + 1$] (for $m \neq j$). Equation (18) calculates the mean relative transition out intensity MRO_m for trend m transitioning to other types.

$$RO_{mj} = \frac{C_{mj}}{\sum_{i \neq m} C_{mi}} \tag{17}$$

$$MRO_m = \frac{1}{I-1}\sum_{j \neq m} RO_{mj} \tag{18}$$

where C_{im} represents the area of the initial vegetation growth trend i transitioning to the final growth trend type m.

3. Results

3.1. Spatiotemporal Variability of Vegetation Cover

3.1.1. Temporal Variation Characteristics

The annual average NDVI values for Liangbei Town from 2000 to 2023 were calculated and denoted as the annual NDVI of Liangbei Town. A trend chart depicting the annual NDVI changes from 2000 to 2023 was created, as shown in Figure 3.

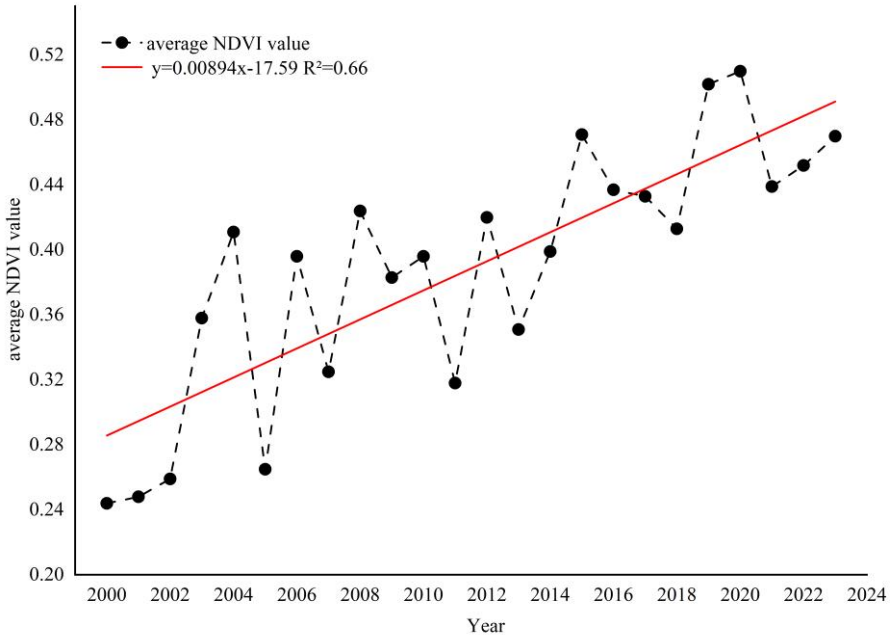

Figure 3. Annual NDVI temporal variation trend of Liangbei Town (2000–2023).

From Figure 3, it can be observed that the NDVI of Liangbei Town ranged between 0.24 and 0.52 during the period from 2000 to 2023, with an average value of 0.38. The linear expression for the time series trend analysis of NDVI in Liangbei Town from 2000 to 2023 is $y = 0.00894x - 17.59$. This indicates an overall increasing trend in the annual NDVI, with a change rate of 0.0894 per decade.

During the period from 2000 to 2023, the years with an increasing NDVI trend include 2000–2001, 2001–2002, 2002–2003, 2003–2004, 2005–2006, 2007–2008, 2011–2012, 2013–2014, 2014–2015, 2018–2019, 2021–2022, and 2022–2023. Notably, the year 2005 to 2006 exhibited the highest growth amplitude (0.231) and growth rate (140%). Conversely, the years with a decreasing NDVI trend include 2004–2005, 2006–2007, 2008–2009, 2010–2011, 2012–2013, 2015–2016, 2016–2017, 2017–2018, and 2020–2021. Among these, the period from 2004 to 2005 experienced the highest decline amplitude (0.246) and a reduction rate of 59.8%.

The LandTrendr algorithm was employed to model the time series curves of NDVI spectral values across three typical land cover types in Liangbei agricultural land, industrial land, and residential land. The results are presented in Figure 4. The "folds" fitted by the LandTrendr algorithm capture sudden changes in the NDVI spectral values at specific points in time within the long-term series.

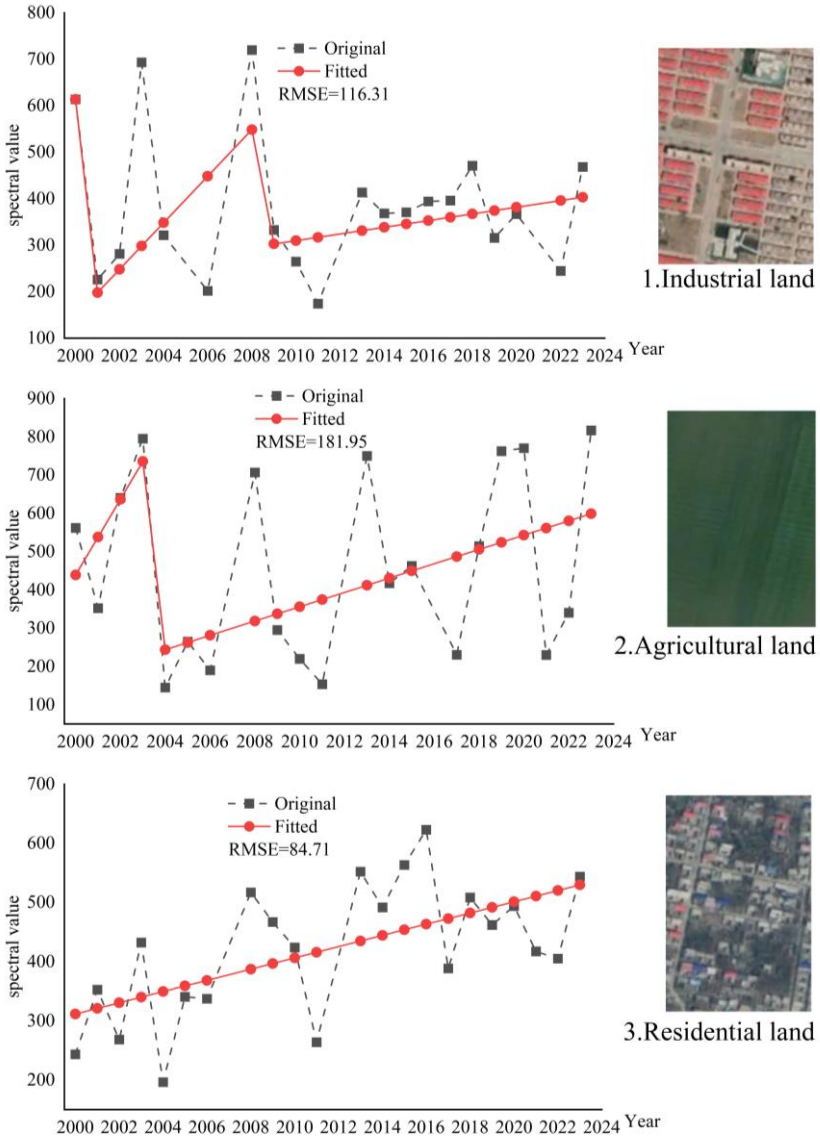

Figure 4. LandTrendr algorithm fitting NDVI spectral values for three typical land types.

For instance, in the spectral curve for industrial land, the fitted line exhibits significant bends in 2001 and 2009, indicating abrupt changes in the NDVI spectral values at these times. Specifically, the trend shifts from a decrease to an increase after 2001, followed by a deceleration in the rate of increase after 2009. Similarly, the spectral curve for agricultural land shows a significant bend in 2004, reflecting a sudden change in spectral values, accompanied by a subsequent slower growth trend. In contrast, the spectral curve for residential land does not show any abrupt changes, and the trend consistently increases over time.

To further pinpoint significant change points in the annual NDVI values for Liangbei from 2000 to 2023, a Mann–Kendall (MK) test was conducted. As illustrated in Figure 5, the test results indicate a critical change point in 2012. The UF curve, representing a standard normal distribution calculated sequentially from the annual NDVI, intersects with the UB curve, derived from the inverse sequence, at this year. Since the intersection occurs within the confidence interval defined by $\alpha = \pm 1.96$, the data pass the 95% significance test, confirming a statistically significant mutation point in 2012.

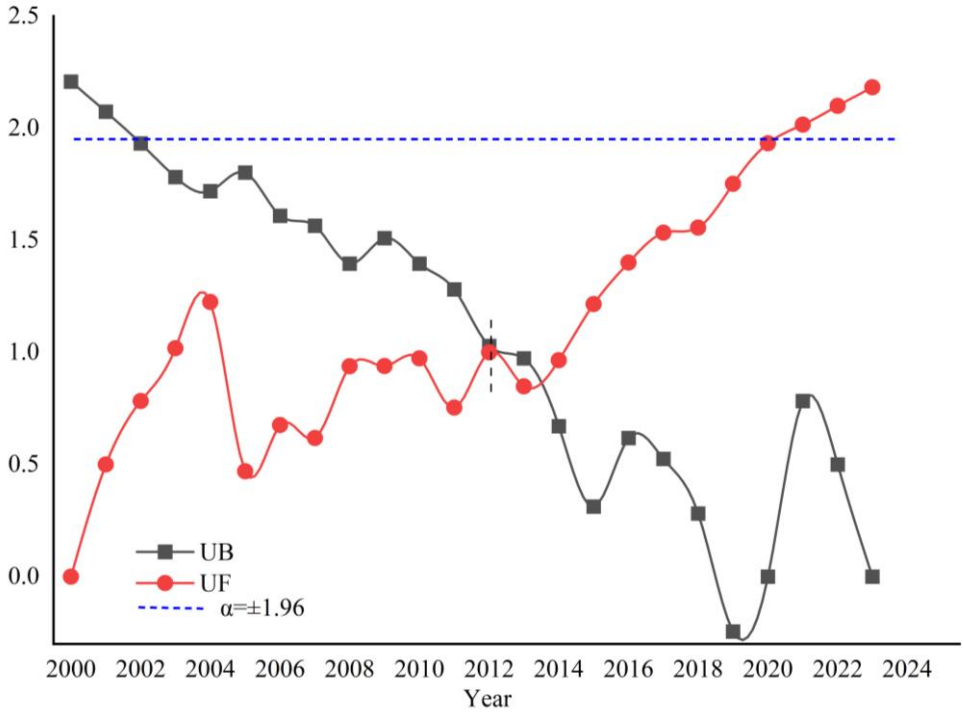

Figure 5. Mann–Kendall Test of Long-Term Sequence.

3.1.2. Spatial Distribution Characteristics

The average NDVI values for Liangbei Town from 2000 to 2023 were calculated on a per-pixel basis, referred to as the annual mean NDVI of Liangbei Town. A spatial distribution map of the annual mean NDVI was then generated, as shown in Figure 6.

According to Figure 6, the annual mean NDVI of Liangbei Town from 2000 to 2023 ranges between 0.12 and 0.51, with an average value of 0.38. The spatial distribution shows significant variability, characterized by higher values on both sides and lower values in the middle. Based on this result, the annual mean NDVI of Liangbei Town from 2000 to 2023 was reclassified into distinct classes with thresholds set at 0.2, 0.3, and 0.4, as illustrated in Figure 6b. The statistical results are presented in Table 1.

Table 1. Area and percentage of NDVI classes.

Class	NDVI Range	Area (km²)	Area Percentage (%)
I	0.12–0.2	0.58	1.24
II	0.2–0.3	7.04	15.15
III	0.3–0.4	15.47	33.28
IV	0.4–0.51	23.41	50.34

Classes I and II combined account for 16.39% of the area, corresponding to 7.62 km^2. These areas are mainly located in the central construction land, including residential areas, roads, and deep mining areas, which have relatively low NDVI values. Class III covers an area of 15.47 km^2, making up 33.28% of the study area. These regions include the green belts around the main channel of the South-to-North Water Diversion Project, parks, and forested areas surrounding arable land. Class IV, with an area of 23.41 km^2 and an area percentage of 50.34%, is the most extensive among all classes. These regions are agricultural land.

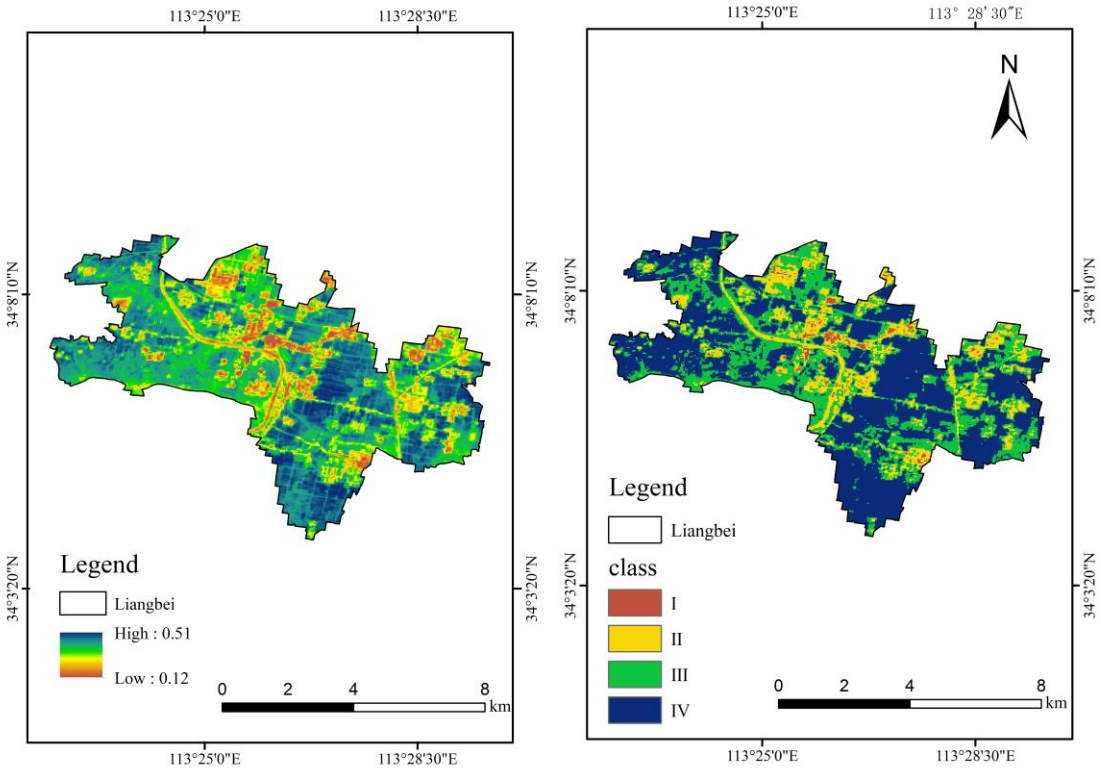

Figure 6. Spatial distribution and classification of annual mean NDVI in Liangbei Town. (**a**) NDVI spatial distribution. (**b**) NDVI classification distribution.

3.1.3. Spatial Variation Characteristics

The coefficient of variation (CV) of NDVI for Liangbei Town from 2000 to 2023 was calculated on a per-pixel basis. Based on the CV, the NDVI in the region was classified into four categories: stable, relatively stable, unstable, and extremely unstable, as shown in Figure 7.

The coefficient of variation for NDVI in Liangbei Town ranges from 0 to 0.87, with an average value of 0.26. The area proportions of the four stability categories are in the order of unstable > extremely unstable > relatively stable > stable. The extremely unstable areas are primarily located in concentration of population and deep mining areas, where human activities significantly influence NDVI fluctuations. The unstable areas are mainly agricultural land, where changes in crop growth, variety, and area affect the NDVI.

By conducting a combined analysis using the Sen slope estimator and the Mann–Kendall (MK) test on the NDVI time series trends for Liangbei Town from 2000 to 2023. This analysis provided insights into the spatial distribution of NDVI trend changes, as depicted in Figure 8.

The slope of the NDVI trend in Liangbei Town ranges from −0.17 to 0.024, with an average value of 0.01, indicating a clear upward trend. The area exhibiting an increasing trend is 42.98 km^2, accounting for 92.42% of the total study area. Conversely, the area showing a degradation trend is 2.86 km^2, or 6.14% of the total area. This indicates that the area with an increasing trend is 15 times larger than that with a degrading trend, demonstrating a steady improvement in vegetation cover and growth in Liangbei Town over the past 24 years.

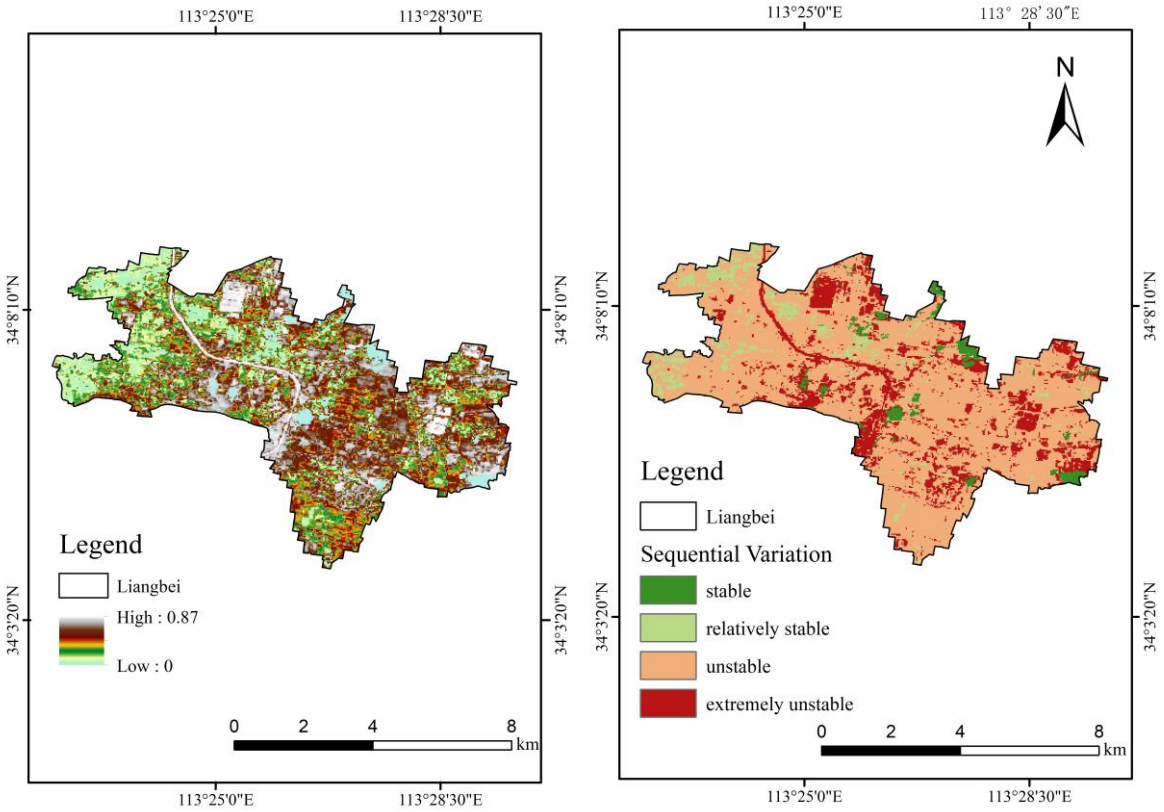

Figure 7. Temporal stability of NDVI in Liangbei Town. (**a**) CV spatial distribution. (**b**) CV classification distribution.

Based on the criteria sen < −0.0005, |Z| > 1.96; sen < −0.0005, |Z| < 1.96; −0.0005 < sen < 0.0005, |Z| < 1.96; sen > 0.0005, |Z| > 1.96; sen > 0.0005, |Z| < 1.96, the NDVI trend was classified into five categories: significant degradation, slight degradation, stable, slight improvement, and significant improvement, respectively. The area and percentage of each category are shown in Table 2.

Table 2. Area and percentage of NDVI trend classes.

Class	Area (km²)	Area Percentage (%)
Significant Degradation	0.99	2.12
Slight Degradation	1.87	4.02
Stable	0.67	1.43
Slight Improvement	4.25	9.14
Significant Improvement	38.73	83.28

The ranking of area proportions is significant improvement (83.28%) > slight improvement (9.14%) > slight degradation (4.02%) > significant degradation (2.12%) > stable (1.43%). The areas of improvement are mainly agricultural lands, attributed to changes in crop growth, increased planting area, and reclamation of wasteland. The degrading areas are primarily in the northeast of Liangbei Town, where urbanization and deep mining have led to significant vegetation degradation and a marked decrease in the NDVI.

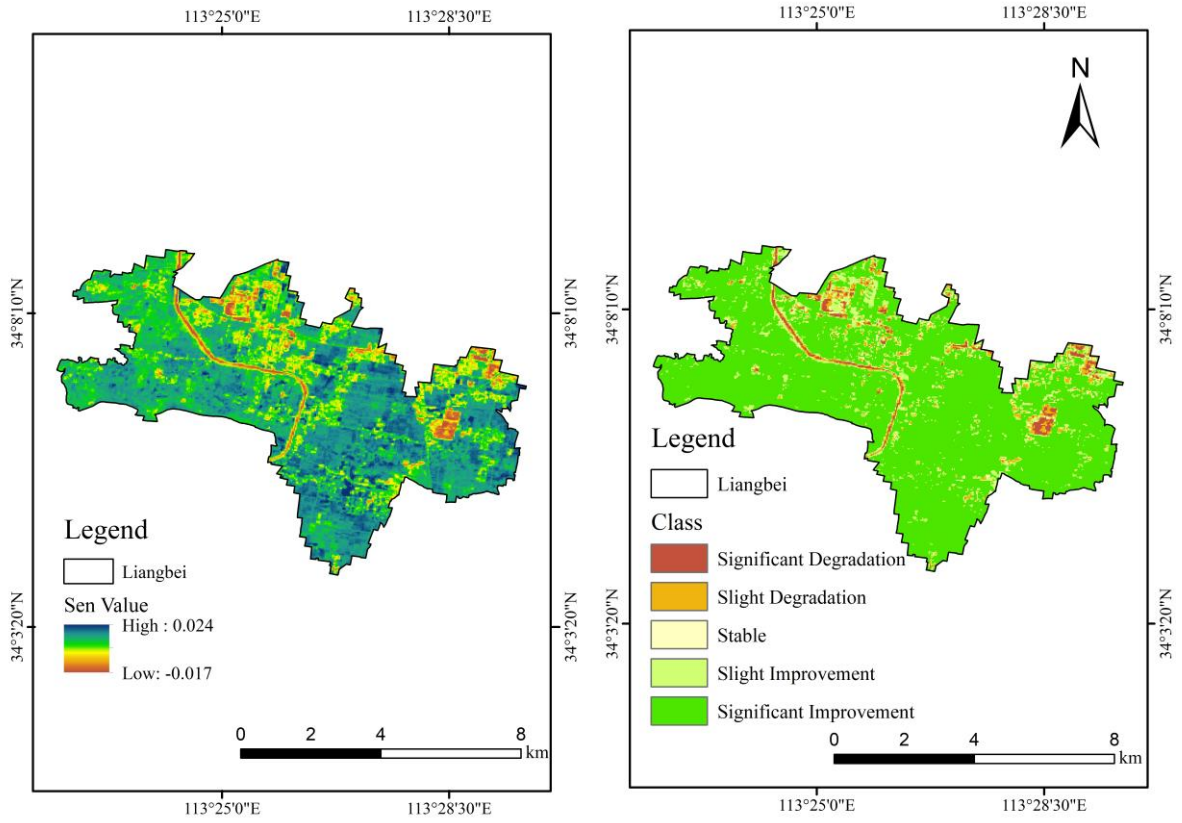

Figure 8. Spatial distribution of NDVI trend changes in Liangbei Town. (**a**) Sen spatial distribution. (**b**) Sen + MK classification distribution.

3.1.4. Future Trend Prediction

The future trend of the NDVI in Liangbei Town was predicted using the Hurst index, and a spatial distribution map was generated, as shown in Figure 9a. The Hurst index ranges from 0.15 to 0.72, with an average value of 0.38. According to the results, the area percentage of regions with persistent change ($0.5 < H < 1$) is 7.31%, while the area percentage of regions with anti-persistent change ($0 < H < 0.5$) is 91.13%. By overlaying the NDVI trend with the Hurst index, a future trend map was produced, as illustrated in Figure 9b, and the corresponding statistics are presented in Table 3.

Table 3. Future NDVI trend classes.

Sen Slope	Hurst Index	Future Trend	Area (km²)	Area Percentage (%)
<0	$0.5 < H < 1$	Continuous decrease	0.75	1.62%
	$0 < H < 0.5$	Transition from decrease to increase	2.38	5.11%
>0	$0 < H < 0.5$	Transition from increase to decrease	40.73	87.58%
	$0.5 < H < 1$	Continuous increase	2.64	5.69%

The analysis results in Figure 9b and Table 3 indicate that the future NDVI trend in Liangbei Town is predominantly characterized by a transition from increase to decrease (87.58%) > continuous increase (5.69%) > transition from decrease to increase (5.11%) > continuous decrease (1.62%). This suggests that the future NDVI of Liangbei Town is expected to shift from increasing to decreasing.

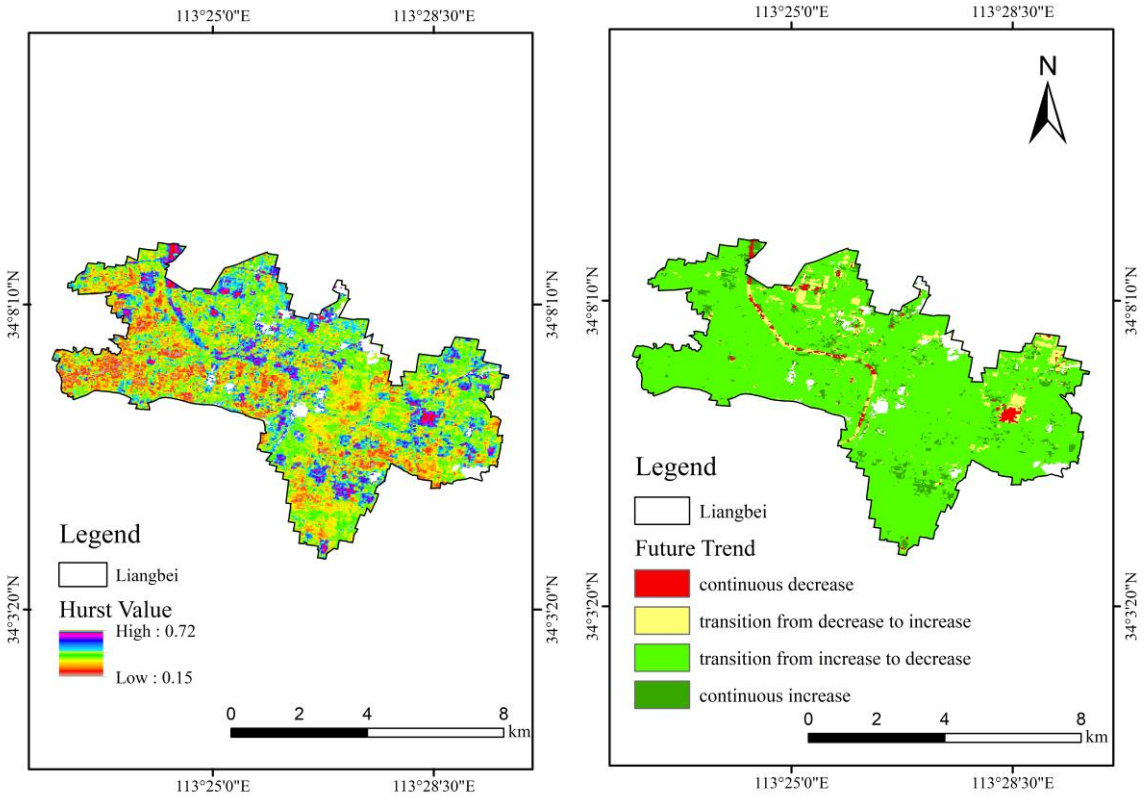

Figure 9. Future NDVI trends in Liangbei Town. (**a**) Hurst spatial distribution. (**b**) Future trend classification distribution.

3.2. Analysis of Vegetation Intensity Changes

3.2.1. Analysis of Vegetation Growth Trend Changes

Based on the Mann–Kendall (MK) test results for the annual NDVI time series, 2012 emerged as a critical change point. Recognizing this mutation point, the study period from 2000 to 2023 was divided into two distinct phases: 2000–2012 and 2012–2023. To further analyze the vegetation evolution trends during these two phases, a transfer matrix was generated using ArcGIS. The results of this transfer matrix, illustrating the shifts in vegetation patterns between the two periods, are presented in Figure 10.

The transfer matrix illustrates the area transitions between different vegetation growth trends across the two phases. During the transition from the first phase (2000–2012) to the second phase (2012–2023), the trend of slight improvement exhibited the highest total transition area of 18.65 km^2. Among these transitions, the most prominent was the shift from slight improvement to significant improvement, covering an area of 10.98 km^2. The overall transitions between vegetation growth trends were relatively straightforward, primarily involving shifts between slight and significant improvement.

To gain deeper insights into these transitions and understand the underlying dynamics, an intensity analysis framework was introduced. This framework allows for the exploration of potential transfer relationships between vegetation growth trends, providing deeper insights beyond the basic transitions observed in the transfer matrix.

Figure 11 illustrates the intensity changes in vegetation growth trends, where the X-axis represents the initial vegetation growth trend, and the Y-axis represents the end vegetation growth trend. Each cell contains four elements: absolute admission intensity, absolute transfer intensity, relative admission intensity, and relative transfer intensity. The filling rules are as follows: blue indicates Inhibitor, and red indicates Tendency.

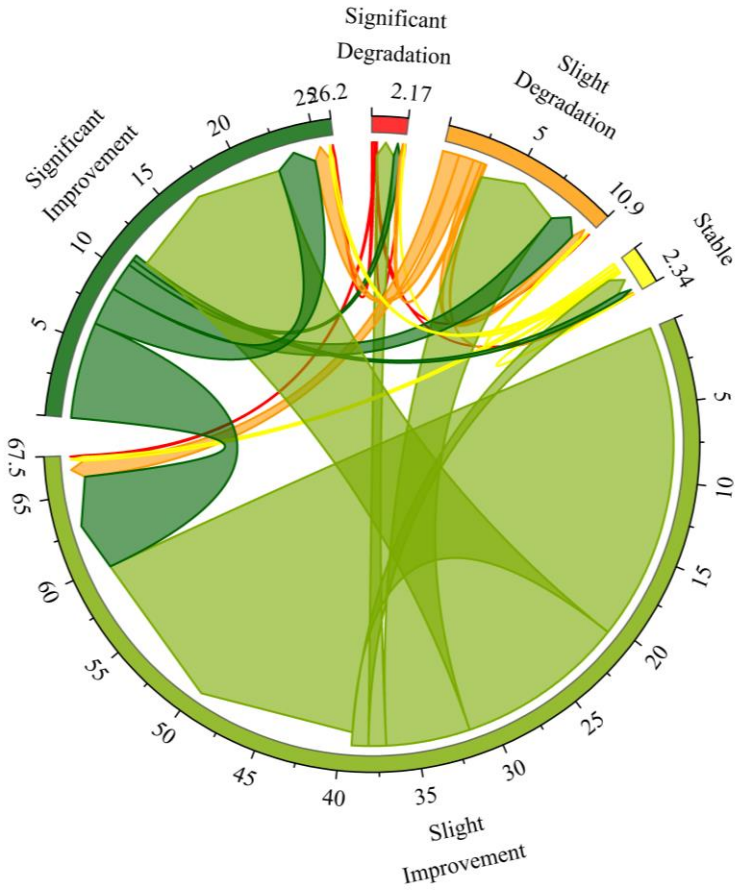

Figure 10. Transfer of vegetation growth trends from 2000−2012 to 2012−2023.

Specifically:

(1) If elements 1 and 2 within a cell are filled with red, it indicates an absolute inclination for the initial vegetation growth trend to transform into the final vegetation growth trend.

(2) If elements 3 and 4 are filled with red, it indicates a relative inclination for the transformation process.

(3) If all elements in a cell are filled with blue, the transformation process is systemically suppressed.

(4) If all elements are filled with red, the transformation process shows a systemic inclination.

This analysis framework helps in understanding the underlying patterns and tendencies in vegetation growth trend transitions, providing a detailed view of how vegetation cover changes over time and how these changes are interconnected. This understanding is crucial for effective management and conservation strategies, especially in regions experiencing significant environmental changes.

Relative Tendency: The transitions such as significant degradation to stable, significant degradation to significant improvement, slight degradation to significant degradation, slight degradation to stable, slight degradation to significant improvement, stable to severe degradation, stable to slight degradation, stable to significant improvement, and significant improvement exhibit relative inclination characteristics.

Absolute Tendency: The transitions such as slight improvement to slight degradation, slight improvement to significant improvement, and significant improvement to slight improvement show absolute inclination characteristics.

Systemic Inhibition: The transition from significant degradation to slight degradation shows systemic suppression characteristics.

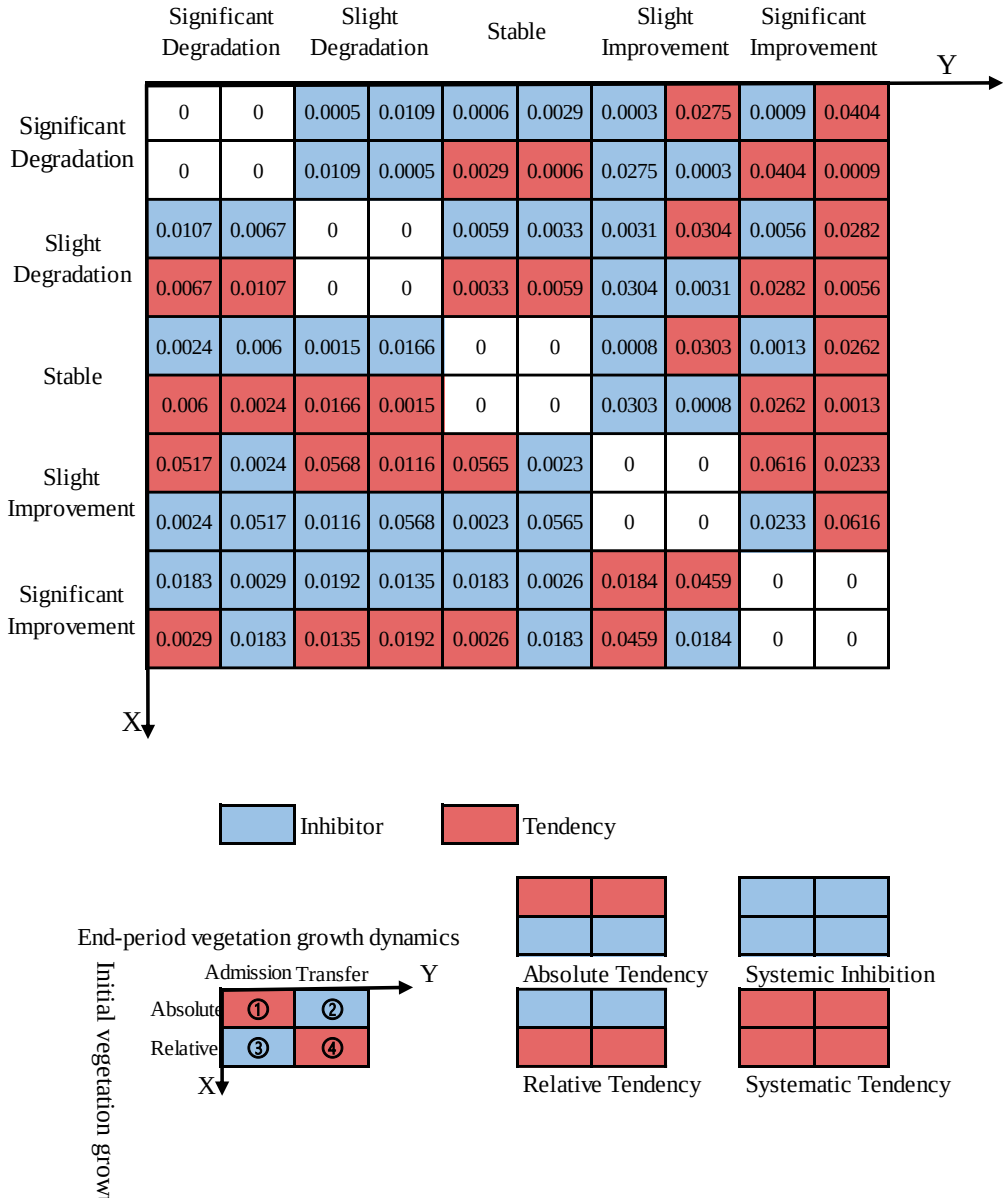

Figure 11. Intensity changes in vegetation growth trends.

3.2.2. Analysis of Slight Improvement to Significant Improvement Change Pattern

The transfer intensity between vegetation growth trends was calculated based on the transition area within the study area. The results are depicted in Figure 12. The red dashed lines in the figure represent the average intensity of either admission or transfer transitions as a percentage. If the transition intensity exceeds the average, it indicates a targeted gain or loss in vegetation growth trend.

Absolute Intensity: (1) The average absolute admission intensity is 0.0056%. The slight improvement trend tends to receive more area from the significant improvement trend at an intensity greater than 0.0056% (Figure 12a). This suggests that the slight improvement trend is more likely to gain area from the significant improvement trend while suppressing gain from other categories. (2) The average absolute transfer intensity is 0.01%, with the slight improvement trend tending to transition to the significant improvement trend at an intensity higher than 0.01% (Figure 12c). This suggests that the slight improvement trend is more inclined to transition to the significant improvement trend.

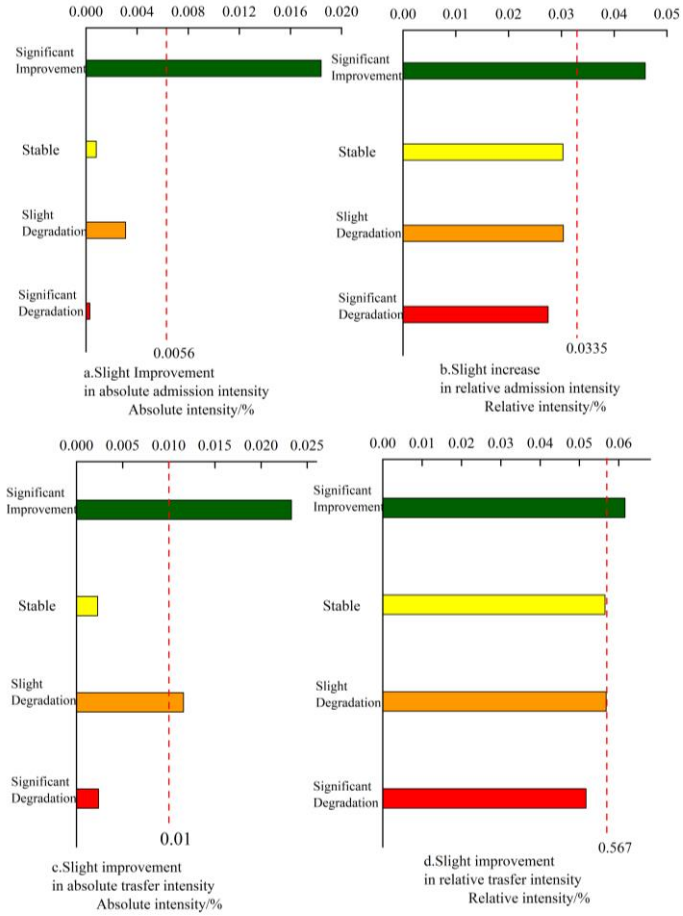

Figure 12. Transition intensity analysis for vegetation growth trends.

Relative Intensity: (1) The average relative admission intensity is calculated to be 0.0335%. The slight improvement trend shows a strong tendency to gain area from the significant improvement trend, with an admission intensity higher than the average. This preference indicates that the transition of areas from significant improvement to slight improvement has a relatively greater impact on the proportion of areas experiencing a slight improvement (Figure 12b). (2) The average relative transfer intensity is calculated to be 0.567%. The slight improvement trend tends to transition into the significant improvement trend with a transfer intensity of 0.061%, which is higher than the average transfer intensity. This indicates a strong propensity for the slight improvement trend to convert into the significant improvement trend, reinforcing the inclination observed in the absolute intensity analysis (Figure 12d).

The combined analysis of absolute and relative intensities provides a comprehensive understanding of the transition patterns between vegetation growth trends. The slight improvement trend, in particular, shows a marked tendency to both receive area from and transition into the significant improvement trend, highlighting a specific directional dynamic within the study area. These insights are critical for developing targeted vegetation management strategies, ensuring effective monitoring, and fostering sustainable land use practices.

3.3. Analysis of Driving Factors

3.3.1. Climate Driving Factors

To explore the impact of climate change on the vegetation in Liangbei Town, we plotted the interannual variation curves of the region's average temperature and average precipitation, as shown in Figure 13.

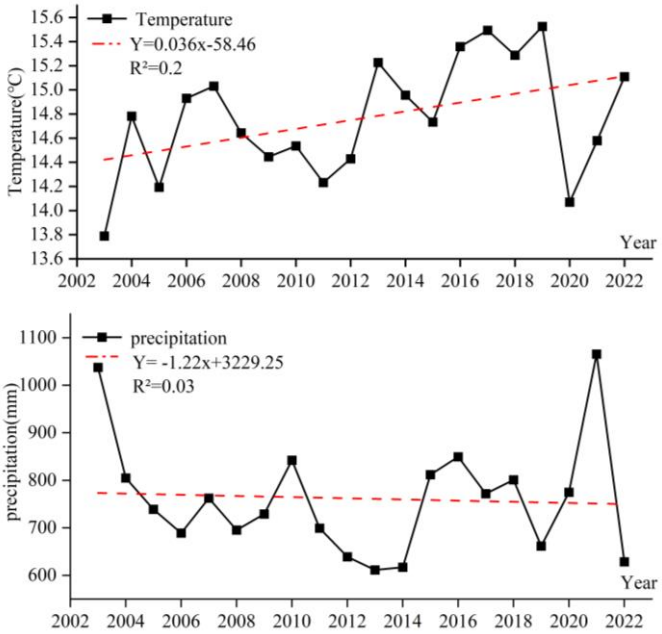

Figure 13. Annual average temperature and precipitation line chart.

Average Temperature: from 2003 to 2022, the multi-year average temperature was 14.76 °C. The highest temperature was 15.52 °C (2019) and the lowest was 13.78 °C (2003). The temperature showed an increasing trend, with an average annual increase of 0.036 °C.

Annual Precipitation: The range of annual precipitation was between 600.2 mm and 1132.8 mm. Annual precipitation showed a decreasing trend, with an average annual decrease of 1.22 mm.

The correlation between annual average temperature, precipitation, and the NDVI was examined using the Pearson correlation coefficient. The results are as follows: (1) The correlation coefficient between annual average temperature and annual average NDVI was 0.17 (p = 0.3). (2) The correlation coefficient between annual average precipitation and annual average NDVI was 0.263 (p = 0.21).

A correlation coefficient value exceeding 0.5 with a p-value less than 0.01 indicates a significant correlation; the larger the correlation coefficient, the stronger the correlation. Neither the annual average temperature nor the annual average precipitation showed a significant correlation with the annual average NDVI, suggesting that climate factors are not the main drivers of NDVI changes in Liangbei Town. This lack of significant correlation may be due to the region having sufficient sunlight and precipitation during the study period, resulting in minimal impact on vegetation growth trends.

3.3.2. Underground Mining Driving Factors

An analysis of ground subsidence in Liangbei Town from 2018 to 2023 was conducted using SAR data. The D-InSAR processing results are shown in Figure 14. For instance, the monitoring focused on mining face 32051, located in the lower part of the east wing of the 32 mining area, near the DF3 fault protection coal pillar to the north. The working face had a designed length of approximately 770 m and a dip of 224 m. The actual mining length was 664 m, with an azimuth angle of 85°33′25″ and an average mining depth of 580 m. Borehole data showed an average coal thickness of 5.04 m, a simple coal seam structure, and a relatively stable coal seam with a dip angle of 6°. Mining operations began in October 2020 and ended in October 2022.

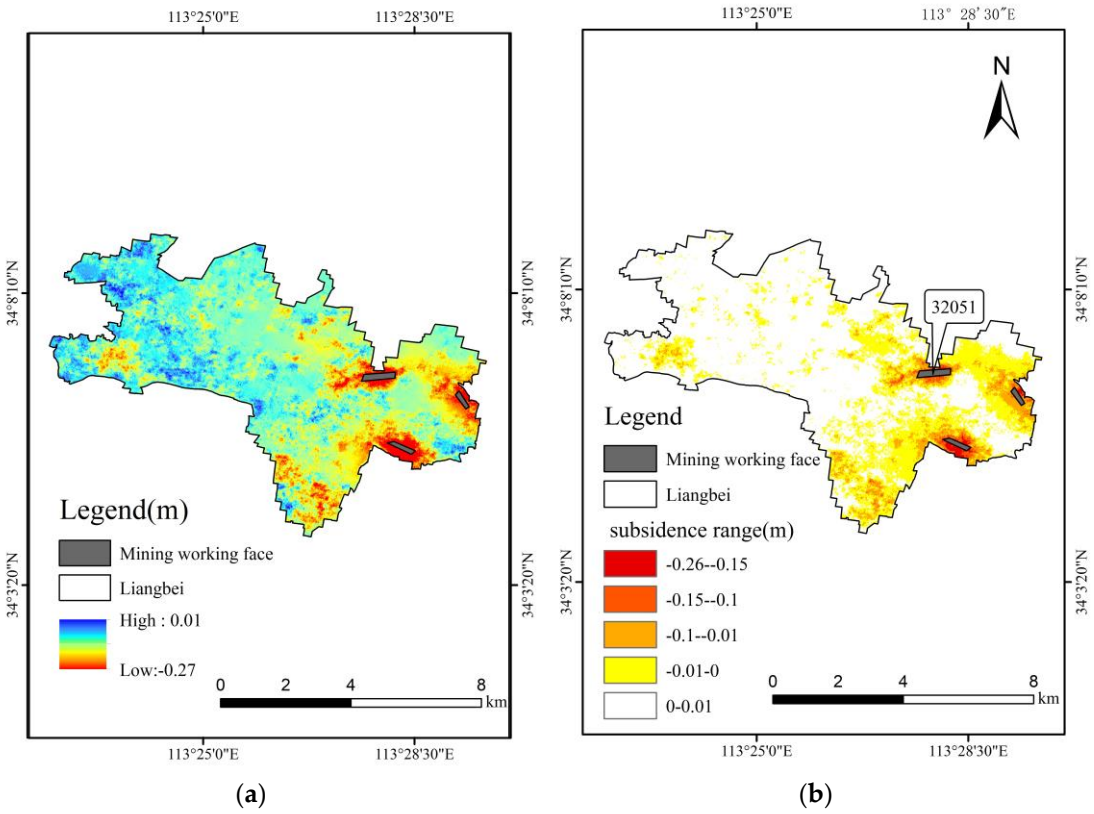

Figure 14. Distribution of ground subsidence in Liangbei Town. (**a**) Spatial distribution. (**b**) Classification distribution.

As shown in Figure 14, ground subsidence in Liangbei Town is predominantly concentrated in the eastern region. The maximum subsidence is 0.26 m, covering an area of 15.66 km^2 (13.67%). The area with ground subsidence between 0.15 m and 0.26 m is 0.32 km^2 (0.69%), and the mining workfaces are mainly distributed in these regions. The area with ground subsidence between 0.1 m and 0.15 m is 0.74 km^2 (1.6%), and the area between 0.01 m and 0.1 m is 2.95 km^2 (6.36%). These areas are distributed around the mining workfaces. The area with ground subsidence between 0 m and 0.01 m is 11.64 km^2 (25.03%). Areas close to the mining workfaces are still affected, while those farther away are mainly affected by surface construction subsidence. The NDVI values for each subsidence range during 2018–2023 are shown in Figure 15.

In areas unaffected by subsidence, NDVI values remain at their highest. However, as ground subsidence intensifies, NDVI values exhibit a gradual decline, reflecting the impact of underground mining activities on surface vegetation. The analysis reveals a clear relationship between subsidence levels and NDVI values:

0–0.01 m Subsidence: NDVI values range from 0.69 to 0.79, with an average of 0.75.

0.01–0.1 m Subsidence: NDVI values range from 0.67 to 0.74, with an average of 0.72.

0.1–0.15 m Subsidence: NDVI values range from 0.65 to 0.72, with an average of 0.69.

0.15–0.26 m Subsidence: NDVI values range from 0.59 to 0.69, with an average of 0.64.

The findings indicate that greater ground subsidence correlates with higher underground mining intensity, leading to more pronounced surface damage and a corresponding reduction in NDVI values. Notably, after the resumption of mining activities in 2020, a decline in NDVI values was observed across all subsidence categories in 2021. The most significant decrease occurred in areas with the highest subsidence, where NDVI values dropped from 0.69 in 2020 to 0.57 in 2021. This trend underscores the substantial impact of increased subsidence on vegetation health.

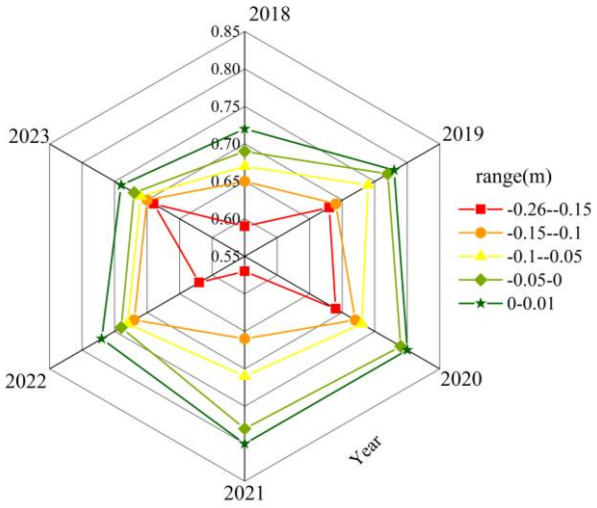

Figure 15. NDVI values in different subsidence areas (2018–2023).

4. Discussion

4.1. Ecological Restoration

Liangbei Town, a critical area for deep mining in central China, has experienced significant surface subsidence due to ongoing extraction activities, especially in the 32051 working face. From 2018 to 2023, the subsidence affected approximately 15.66 km^2, predominantly in the eastern region of the town. This study reveals that despite these substantial mining activities, the annual vegetation dynamics in Liangbei Town exhibit a notable upward trend, with a significant NDVI increase observed across 38.73 km^2 between 2000 and 2023.

The upward trend in vegetation suggests that both natural and artificial ecological restoration efforts have played crucial roles in mitigating the adverse effects of deep mining on surface vegetation. These findings are consistent with previous research by Xiao Wu et al. [48], which showed that the relationship between mining intensity and ecosystem services is not linear. The flat terrain and favorable hydrothermal conditions in Liangbei make it well-suited for crops such as wheat. This study shows that the interplay between human intervention and natural recovery processes can contribute to vegetation resilience, even under high-intensity coal mining activities. The combination of natural succession and targeted restoration efforts may have prevented severe degradation, underscoring the importance of integrated ecological management in mining regions.

4.2. Future Trends and Challenges

The areas of continuous NDVI decrease are mainly located in the northeastern part of Liangbei, which are deep mining areas where continuous surface vegetation destruction leads to persistent NDVI decline. Although the macro-level analysis shows no significant decline in surface vegetation, the Hurst index analysis reveals that 91.13% of the vegetation in Liangbei is projected to experience anti-persistent changes, suggesting potential future instability. The saturation of crop planting conditions in agricultural areas is a primary driver of this trend, indicating that the existing agricultural practices may have reached their ecological capacity.

Areas with continuous NDVI decline, particularly in the northeastern part of Liangbei Town, are closely associated with deep mining activities. These regions exhibit persistent vegetation degradation, likely due to ongoing surface deformation and soil destabilization caused by subsidence. Managing the delicate balance between mining activities and environmental protection remains a critical challenge. In ecologically sensitive areas, minimizing artificial intervention and allowing for natural recovery, as advocated by Hu Zhenqi et al. [49], could offer a pathway toward achieving ecological equilibrium.

4.3. Managing Mining-Induced Subsidence

The negative impacts of mining-induced subsidence on surface vegetation highlight the need for carefully planned remediation measures. Effective ecological restoration in subsidence areas should be informed by up-to-date land use planning, ensuring that restoration activities align with local environmental conditions and socio-economic needs. Afforestation, sustainable agriculture, or adaptive construction practices can help mitigate the ecological damage caused by subsidence, but these approaches must be tailored to the specific conditions of each affected area.

Previous studies [50] have emphasized the importance of controlling the width of the working face and the rate of advance during mining operations, as these factors significantly influence the extent of overburden damage. Optimizing these parameters can reduce surface disturbance and promote more effective post-mining ecological restoration. However, the focus on deep-seam mining raises questions about the broader applicability of these findings. The surface environmental evolution observed in Liangbei Town may differ from that in areas affected by shallow mining, where the dynamics of subsidence and vegetation recovery could follow different patterns.

4.4. Study Advantages and Limitations

This research contributes to the understanding of vegetation dynamics in deep mining areas, providing a detailed analysis of both temporal and spatial changes in NDVI. The integration of remote sensing data with advanced analytical techniques, such as LandTrendr algorithm, Sen's slope, the Mann–Kendall test, and intensity analysis, offers a comprehensive approach to monitoring vegetation in mining regions. However, this study is limited by its focus on deep-seam mining, which may not fully capture the complexity of vegetation responses in areas subjected to different mining intensities or methods. Future research should consider comparative studies between deep and shallow mining regions to enhance our understanding of the environmental impacts across varying mining contexts.

In conclusion, while this study underscores the resilience of vegetation in Liangbei Town under deep mining pressures, it also highlights the ongoing challenges in balancing resource extraction with ecological sustainability. The findings serve as a foundation for future research and management strategies aimed at mitigating the environmental impacts of mining in similar regions.

5. Conclusions

This study reveals a clear upward trend in vegetation cover in Liangbei from 2000 to 2023, despite high-intensity coal mining activities. Key findings include:

(1) Temporal Dimension: The annual NDVI increased at a rate of 0.0894 $(10a)^{-1}$, peaking at 0.51 in 2020, with the most rapid growth occurring between 2005 and 2006 (140% increase).
(2) Spatial Dimension: NDVI values were lower in the center and higher around the edges, with cultivated land covering 50.34% of the area showing NDVI values between 0.4 and 0.51.
(3) Trend of Change: Significant NDVI improvement was observed in 83.28% of the area, with a notable transition from slight to significant improvement over 10.98 km^2, indicating broad regional vegetation recovery.
(4) Driving Factors: Deep mining in the eastern region led to a maximum ground subsidence of 0.26 m over 15.66 km^2, corresponding to a decrease in the NDVI within affected areas.

These results underscore the importance of balancing mining and environmental protection for sustainable ecosystem development, with implications for future management strategies.

Author Contributions: Conceptualization, Z.C. and W.Y.; methodology, Z.C.; software, Z.C. and C.Z.; validation, Z.C.; formal analysis, Z.C.; investigation, Z.C.; resources, Z.C.; data curation, Z.C.; writing—original draft preparation, Z.C.; writing—review and editing, Z.C. and C.Z.; visualization, Z.C.; supervision, J.C.; project administration, J.C.; funding acquisition, W.Y. All authors have read and agreed to the published version of the manuscript.

Funding: This research was funded by the National Natural Science Foundation of China: (42207534, U21A20108), Natural Science Foundation of Henan Province: (242300421363), Excellent Youth Foundation of Henan Polytechnic University: (J2024-4), Training Plan for Young Backbone Teachers in Higher Education Institutions in Henan Province (2024GGJS038).

Data Availability Statement: Landsat 5/7/8, sourced from the United States Geological Survey USGS (https://www.usgs.gov/, accessed on 27 May 2024), Google Earth Engine (https://earthengine.google.com/, accessed on 27 May 2024).

Conflicts of Interest: The authors declare no conflicts of interest.

References

1. Chao, J.; Liu, S.; Hu, D.; Han, X.; Yu, M.; Pan, R. Early Prediction and Forecasting Methods of Coal Spontaneous Combustion in Deep Goaf Areas. *J. Henan Polytech. Univ.* **2024**, *43*, 34–41. (In Chinese)
2. Lin, B.; Yang, W.; Liu, T. Typical Characteristics, Triggering Mechanisms, and Control Strategies of High Bump Risk Coal Seams in Deep Mining. *J. China Coal Soc.* **2024**. (In Chinese) [CrossRef]
3. Wang, W.; Liu, R.; Gan, F.; Zhou, P.; Zhang, X.; Ding, L. Monitoring and Evaluating Restoration Vegetation Status in Mine Region Using Remote Sensing Data: Case Study in Inner Mongolia, China. *Remote. Sens.* **2021**, *13*, 1350. [CrossRef]
4. Song, W.; Song, W.; Gu, H.; Li, F. Progress in the Remote Sensing Monitoring of the Ecological Environment in Mining Areas. *Int. J. Environ. Res. Public Health* **2020**, *17*, 1846. [CrossRef] [PubMed]
5. Wang, S.; Huang, Q.; Fan, L.W. Ecological Development and Ecological Water Level Protection in Ecologically Fragile Areas with Coal Mining. *Coal Geol. China* **2011**, *23*, 31.
6. Li, S.; Li, X.; Men, L.; Zhao, H.; Guo, X. Zoning and Planning of Direction for Reclamation of Subsidence Areas in High Water-Level Plains Mining Area. *J. Coal Sci. Technol.* **2020**, *48*, 60–69. (In Chinese)
7. Yue, H.; Liu, Y.; Zhu, R. Monitoring Ecological Environment Changes in Shendong Mining Area Based on Remote Sensing Ecological Index. *Bull. Soil Water Conserv.* **2019**, *39*, 101–107.
8. Hu, H.; Lian, X.; Cai, Y.; Zhang, K. Study on Ecological Environment Destruction and Restoration in Shanxi Loess Hilly Coal Mining Subsidence Areas. *J. Coal Sci. Technol.* **2020**, *48*, 70–79. (In Chinese)
9. Zhang, B.; Wu, S.; Ding, X.; Wang, C.; Zhu, J.; Li, Q. Use of Multiplatform SAR Imagery in Mining Deformation Monitoring with Dense Vegetation Coverage: A Case Study in the Fengfeng Mining Area, China. *Remote. Sens.* **2021**, *13*, 3091. [CrossRef]
10. Zhang, X.; Zhou, Y.; Long, L.; Hu, P.; Huang, M.; Chen, Y.; Chen, X. Prediction of the spatiotemporal evolution of vegetation cover in the Huainan mining area and quantitative analysis of driving factors. *Environ. Monit. Assess.* **2023**, *195*, 776. [CrossRef]
11. Sun, X.; Yuan, L.; Liu, M.; Liang, S.; Li, D.; Liu, L. Quantitative estimation for the impact of mining activities on vegetation phenology and identifying its controlling factors from Sentinel-2 time series. *Int. J. Appl. Earth Obs. Geoinf.* **2022**, *111*, 102814. [CrossRef]
12. Hui, J.; Chen, Z.; Ye, B.; Shi, C.; Bai, Z. Remote Sensing Monitoring of the Spatial Pattern of Greening and Browning in Xilin Gol Grassland and Its Response to Climate and Human Activities. *Remote. Sens.* **2022**, *14*, 1765. [CrossRef]
13. Liu, Y.; Lei, S.; Chen, X.; Chen, M.; Yang, Y.; Li, X.; Zhang, X.; Long, L.; Bian, Z. Analysis of Temporal Variation and Driving Factors of Vegetation Coverage in Shendong Mining Area and Guiding Restoration Strategies. *J. China Coal Soc.* **2021**, *46*, 3319–3331.
14. Yang, Z.; Shen, Y.; Li, J.; Jiang, H.; Zhao, L. Unsupervised monitoring of vegetation in a surface coal mining region based on NDVI time series. *Environ. Sci. Pollution. Res.* **2022**, *29*, 26539–26548. [CrossRef]
15. Ding, Y.; Peng, S.; Du, W. Ecological disturbance effects of surface vegetation during coal mining in arid regions of Western China. *Environ. Monit. Assess.* **2024**, *196*, 498. [CrossRef] [PubMed]
16. Li, H.; Xie, M.; Wang, H.; Li, S.; Xu, M. Spatial Heterogeneity of Vegetation Response to Mining Activities in Resource Regions of Northwestern China. *Remote. Sens.* **2020**, *12*, 3247. [CrossRef]
17. Ma, B.; Yang, X.; Yu, Y.; Shu, Y.; Che, D. Investigation of Vegetation Changes in Different Mining Areas in Liaoning Province, China, Using Multisource Remote Sensing Data. *Remote. Sens.* **2021**, *13*, 5168. [CrossRef]
18. Zhou, B.; Li, H.; Xu, F. Analysis and discrimination of hyperspectral characteristics of typical vegetation leaves in a rare earth reclamation mining area. *Ecol. Eng.* **2022**, *174*, 106465. [CrossRef]
19. Chen, Z.; Zhang, X.; Jiao, Y.; Cheng, Y.; Zhu, Z.; Wang, S.; Zhang, H. Investigating Spatiotemporal Pattern Evolution Characteristics of Vegetation Change in Shendong Coal Mining Area Based on kNDVI and Intensity Analysis. *Front. Ecol. Evol.* **2023**, *11*, 1344664. [CrossRef]
20. Jiang, Q.; Tang, Z.; Zhou, L.; Hu, G.; Deng, G.; Xu, M.; Sang, G. Mapping Paddy Rice Planting Area in Dongting Lake Area Combining Time Series Sentinel-1 and Sentinel-2 Images. *Remote. Sens.* **2023**, *15*, 2794. [CrossRef]

21. Tang, Z.; Ma, J.; Peng, H.; Wang, S.; Wei, J. Spatiotemporal changes of vegetation and their responses to temperature and precipitation in upper Shiyang river basin. *Adv. Space Res.* **2017**, *60*, 969–979. [CrossRef]
22. Liu, R.; Zhu, D. Discussion on Information Mining Method of Land Use Change Based on Transfer Matrix. *Resour. Sci.* **2010**, *32*, 1544–1550.
23. Li, T.; Wu, M.; Duan, C.; Li, S.; Liu, C. The Effect of Different Restoration Approaches on Vegetation Development in Metal Mines. *Sci. Total. Environ.* **2022**, *806*, 150626. [CrossRef] [PubMed]
24. Jia, T.; Hu, X. The Spatiotemporal Evolution Characteristics of Ecological Barrier Areas in China's "Two Splits and Three Belts" from 1985 to 2020. *Bull. Soil Water Conserv. Res.* **2024**, *31*, 348–363. (In Chinese)
25. An, L.; Zhu, J.; Deng, F. Research on Changes in Impermeable Surface in Guiyang City from 1990 to 2020. *J. Hebei Univ. Geol.* **2024**, *47*, 59–66. (In Chinese)
26. Zhao, C.; Qin, Q.; Wu, Z. Consistency Analysis and Correction of Land Surface Reflectance and Vegetation Index of Landsat 5 MSS and TM. *Sci. Geogr. Sin.* **2023**, *43*, 1078–1087. (In Chinese)
27. Lu, X.; Xu, C.; Guo, J. Comparative Analysis of Surface Temperature Retrieval Methods Based on Landsat 8 Data. *Arid Envi-Ronmental Monit.* **2023**, *37*, 137–144. (In Chinese)
28. Ouyang, X.; Zhang, X.; Li, W.; Liu, J.; Liu, Z. Identification of Abandoned Land in Guizhou City Based on Time-Series Data of Sentinel-2 and Landsat Satellites. *Bull. Surv. Mapp.* **2023**, *8*, 57–62. (In Chinese) [CrossRef]
29. Qiu, S.; Zhu, Z.; Olofsson, P.; Woodcock, C.E.; Jin, S. Evaluation of Landsat image compositing algorithms. *Remote. Sens. Environ.* **2023**, *285*, 113375. [CrossRef]
30. Liu, X.; Zhao, C.; Li, B.; Wang, E.; Zhang, Q.; Gao, Y.; Chen, L.; Wang, B.; Hao, J.; Yang, J. Identification and Dynamic Deformation Monitoring of Active Landslides in Gansu Jishishan Earthquake Area Based on InSAR Technology. *J. Wuhan Univ.* **2024**. (In Chinese) [CrossRef]
31. Ma, Z. Study on Key Algorithms of Long-Term Sentinel-1 InSAR Deformation Monitoring. *Acta Geod. Et Cartogr. Sin.* **2024**, *53*, 397.
32. Zhang, F.; Chang, L.; Xun, Z. Ground Deformation Monitoring of Yanghuopan Mining Area Based on SBAS-InSAR Technol-ogy. *China Min.* **2024**, *33*, 152–159.
33. Zhang, Y.; Chen, G.; Ma, Y.; Hu, J.; Ma, Y.; Zhang, L. Research on Surface Melting Change of Mountain Glaciers Based on Sentinel-1 Time-Series Data—Taking Glacier No. 12 in Laohugu as an Example. *Acta Ecol. Sin.* **2024**, *44*, 1389–1403.
34. Feng, H.; Zhao, F.; Wang, Y.; Yan, Y.; Peng, K. Surface Deformation Monitoring of Shanghai Pudong Airport Based on Polarization Time-Series InSAR Technology. *J. Remote Sens.* **2022**, *26*, 2531–2541.
35. Ming, X.; Tian, Y.; Zhang, Q.; Tao, J.; Zhang, Y.; Lin, J. Monitoring and Analysis of Ground Subsidence in Qinfang District Based on Sentinel-1A. *Remote Sens. Nat. Resour.* **2024**, *36*, 35–48.
36. Peng, W.; Kuang, T.; Tao, S. Quantifying influences of natural factors on vegetation NDVI changes based on geographical detector in Sichuan, western China. *J. Clean. Prod.* **2019**, *233*, 353–367. [CrossRef]
37. Kennedy, R.E.; Yang, Z.; Gorelick, N.; Braaten, J.; Cavalcante, L.; Cohen, W.B.; Healey, S. Implementation of the LandTrendr Algorithm on Google Earth Engine. *Remote Sens.* **2018**, *10*, 691. [CrossRef]
38. Fan, Y.; Liu, Y.; Heng, W.; Yue, H.; Bi, Y. Impact analysis of coal mining on ecological environment in Shendong Mining area from 1990 to 2022 based on RSEI. *J. Green Mine.* **2024**, *2*, 41–53. (In Chinese)
39. Ayari, E.; Kassouk, Z.; Lili-Chabaane, Z.; Ouaadi, N.; Baghdadi, N.; Zribi, M. NDVI estimation using Sentinel-1 data over wheat fields in a semiarid Mediterranean region. *GIScience Remote. Sens.* **2024**, *61*, 2357878. [CrossRef]
40. Deng, M.; Jiang, F.; Long, Y.; Wang, T.; Sun, Y. Analysis of Dynamic Changes and Spatial Patterns of Vegetation NDVI in Shenmu City. *J. Cent. South Univ. For. Technol.* **2023**, *43*, 109–119. (In Chinese)
41. Huang, H.; Jin, Y.; Sun, W.; Gao, Y.; Sun, P.; Ding, W. Biomass Burning in Northeast China over Two Decades: Temporal Trends and Geographic Patterns. *Remote. Sens.* **2024**, *16*, 1911. [CrossRef]
42. Lv, G.; Li, X.; Fang, L.; Peng, Y.; Zhang, C.; Yao, J.; Ren, S.; Chen, J.; Men, J.; Zhang, Q.; et al. Disentangling the Influential Factors Driving NPP Decrease in Shandong Province: An Analysis from Time Series Evaluation Using MODIS and CASA Model. *Remote. Sens.* **2024**, *16*, 1966. [CrossRef]
43. Garajeh, M.K.; Akbari, R.; Chaleshtori, S.A.; Abbasi, M.S.; Tramutoli, V.; Lim, S.; Sadeqi, A. A Comprehensive Assessment of Climate Change and Anthropogenic Effects on Surface Water Resources in the Lake Urmia Basin, Iran. *Remote. Sens.* **2024**, *16*, 1960. [CrossRef]
44. Jin, L.; Chen, S.; Yang, H.; Zhang, C. Evaluation and Drivers of Four Evapotranspiration Products in the Yellow River Basin. *Remote. Sens.* **2024**, *16*, 1829. [CrossRef]
45. Ma, Y.; Luo, Y.; Zhong, C.; Yi, W.; Wang, J. Improved Hurst exponent based on genetic algorithm in schizophrenia EEG. *AIP Adv.* **2023**, *13*, 125316. [CrossRef]
46. Ren, F.; Xu, J.; Wu, Y.; Li, T.; Li, M. Analysis of Eco-Environmental Quality of an Urban Forest Park Using LTSS and Modified RSEI from 1990 to 2020—A Case Study of Zijin Mountain National Forest Park, Nanjing, China. *Forests* **2023**, *14*, 2458. [CrossRef]
47. Raubitzek, S.; Corpaci, L.; Hofer, R.; Mallinger, K. Scaling Exponents of Time Series Data: A Machine Learning Approach. *Entropy* **2023**, *25*, 1671. [CrossRef]
48. Xiao, W.; Zhang, W.; Lv, X.; Wang, X. Spatial and Temporal Changes of Ecosystem Services under Different Mining Intensities in Fragile Ecological Areas in Western China—A Case Study of Shenfu Mining Area. *J. Nat. Resour.* **2020**, *35*, 68–81. (In Chinese)

49. Hu, Z.; Wang, J.; Yang, C.; Han, Y.; Peng, P. Analysis of Land Dynamic Change in Yulin Area Based on RS and GIS. *J. Soil Water Conserv.* **2008**, *4*, 82–85. (In Chinese)
50. Zhu, Q.; Li, H.; Yang, X.; Shen, Y. Analysis of Overburden Structure Evolution Characteristics and Its Influence on Surface Sub-sidence. *J. China Coal Soc.* **2019**, *44*, 9–17. (In Chinese)